DEUTSCHES ELEKTRONEN-SYNCHROTRON DESY

DESY 65/15
November 1965
Experimente

HIGHLY POLARIZED COHERENT BREMSSTRAHLUNG FROM A DIAMOND TARGET IN THE GEV REGION

by

G. Bologna
G. Lutz
H. D. Schulz
U. Timm
W. Zimmermann

2 HAMBURG 52 · NOTKESTIEG 1

HIGHLY POLARIZED COHERENT BREMSSTRAHLUNG FROM A DIAMOND TARGET IN THE GEV REGION

by

G.Bologna*
G. Lutz
H.D. Schulz
U. Timm
W. Zimmermann

---

*) On visit from Laboratori Nazionali, CNEN, Frascati, Roma.

Abstract

The production of coherent bremsstrahlung from a crystalline target has been discussed by several authors[1) 2) 3) 4)]. Experimental results were first obtained for 1 Gev with a diamond by Barbiellini et al[5)], who explained the sharp discontinuities of the spectra by taking into account the actual structure of the reciprocal lattice.

We report here on bremsstrahlung spectra obtained from a diamond radiator at an electron energy of 4.8 Gev. The work has essentially two results: (1) The exponentially screened potential of the C atom which has been used earlier[5)] in calculating the bremsstrahlung cross section is not consistent with the experimental spectra. Instead we used a Hartree type screening potential which fits the data very well. (2) The linear polarization obtained from the first peak in a spectrum is much increased, if the orientation of the primary electron momentum is chosen to lie not in the fundamental reference planes of the crystal but at a small angle to one of them.

The production of coherent bremsstrahlung from a crystalline target has been discussed by several authors[1) 2) 3) 4)]. Experimental results were first obtained for 1 Gev with a diamond by Barbiellini et al[5)], who explained the sharp discontinuities of the spectra by taking into account the actual structure of the reciprocal lattice.

We report here on bremsstrahlung spectra obtained from a diamond radiator at an electron energy of 4.8 Gev. The work has essentially two results: (1) The exponentially screened potential of the C atom which has been used earlier[5)] in calculating the bremsstrahlung cross section is not consistent with the experimental spectra. Instead we used a Hartree type screening potential which fits the data very well. (2) The linear polarization obtained from the first peak in a spectrum is much increased, if the orientation of the primary electron momentum is chosen to lie not in the fundamental reference planes of the crystal but at a small angle to one of them.

To illustrate these results we show two types of spectra:

When the primary electron beam was oriented in either one of the fundamental planes (110), (001), or (110), ($1\bar{1}0$) of the crystal lattice with a small angle Θ against the axis (110), we observed spectra with a number of quasi lines, similar to those that had been observed by Barbiellini et al[5)] at 1 Gev. The theoretical polarization of the first peak in these spectra is of the order of 50% and lower.

We found, however, that a much higher polarization could be obtained with a different orientation. We chose a relatively large Θ and turned the electron beam by a small azimuthal angle α against one of these planes. In this case, the spectrum displayed one discontinuity only, all the others remaining small. This is due to the contribution of a single inverse lattice point, as will be shown. The theoretical polarization in this peak is now of the order of 75% and higher, depending on the electron energy and orientation.

We give experimental results for such spectra under four different

conditions of orientation, two for each type, taken with the first peak at 1.44 Gev. These results were obtained from a diamond single crystal at room temperature mounted in the vacuum chamber of the DESY electron synchrotron. The experimental results are compared with the theoretical calculations.

In our experimental arrangement the γ-ray from the diamond radiator passed from the outlet chamber into air through a thin Ti-foil of 10^{-3} rad.lengths. It was then collimated at a distance of 10.5 m from the radiator by a 2x2 mm aperture in a lead block. The collimator was followed by a broom magnet, where the photon beam again entered into a vacuum of 10^{-2} Torr through a Ti-foil of 10^{-3} rad.lengths. In the subsequent vacuum pipe the beam penetrated the shielding wall between synchrotron tunnel and experimental hall. It was further cleaned by a permanent broom magnet of 60000 T. cm, then entered a pair-spectrometer magnet at 28.5 m, and was finally buried in a quantameter at 70 m distance from the radiator.

The thickness of the converter in the pair spectrometer could be chosen between 10^{-4} and 10^{-3} rad.lengths Al or Au, according to experimental conditions of the beam and counter frequency. The spectrometer detected symmetrical and unsymmetrical electron pairs by virtue of four suitably arranged counter telescopes with an energy resolution of 2% in each counter. Prompt and delayed coincidences were recorded.

The single crystal used as radiator was a diamond having the shape of a 1 x 4 x 7 mm^3 parallelepiped. The widest face of it was perpendicular to the (110) axis of the lattice frame. The thickness in the direction of the beam, 1 mm, was equivalent to 0.008 rad.lengths. The diamond was mounted in a remotely controlled goniometer, placed into a straight section of the synchrotron. The crystal could be rotated around a vertical and a horizontal axis, both perpendicular to the beam. The available range of angles Θ_V and Θ_H was $\pm$ 50 mrad. The crystal axes $b_3 = (1\bar{1}0)$, $b_2 = (001)$ were placed parallel to the vertical and horizontal axes of rotation, respectively. The axis $b_1 = (110)$ was therefore parallel to the incident electron beam within $\pm$ 50 mrad. The exact position of the crystal axes

with respect to the electron beam in the coordinate system of the angles of rotation, Θ_V and Θ_H, can be determined by observation of the characteristic dependence of intensity on Θ_V, Θ_H. The angles could be reproduced with an accuracy of better than 0.1 mrad.

The diamond was of a light yellow colour. It turned green where the electron beam hit the crystal. The target spot had an extension of 0.5 mm in the vertical and 2.0 mm in the horizontal direction, the horizontal extension being due to multiple traversals of electrons in the synchrotron. The acceptance defined by the 2 x 2 collimator was therefore $\pm$ 0.125 mrad and $\pm$ 0.2 mrad in the vertical and horizontal directions, respectively. The natural γ-ray cone at 4.8 Gev is $\pm$ 0.106 mrad wide, but this distribution is averaged by multiple scattering of $\pm$ 0.25 mrad in the target, and by the primary divergence of the electron beam, which is not well known but seems to be of the order of $\pm$ 0.1 mrad. The photon intensity is, therefore, approximately integrated over the emission angles of photons with respect to the axis of collimation. The γ-ray intensity after collimation as monitored by a Wilson quantameter is about 10^{10} equivalent quanta per minute. The total intensity which is thus monitored depends on E_o and on the angles of orientation, θ, α, which are defined as follows:

$\theta = \sphericalangle \vec{p}_o$, (110) is defined as the angle between the direction of the primary electron momentum and $\vec{b}_1$. α is the azimuthal angle between the planes $\vec{p}_o$, (110) and (001), (110) (see Fig. 1).

Fig. 1 shows the orientation of $\vec{p}_o$ with respect to the reciprocal lattice frame b_1, b_2, b_3. The indicated structure of the reciprocal lattice plane b_2, b_3 is the same as given in ref.[5]. The triangles, solid and dashed lines, show the intersection of the "pancake region" which has been introduced by Überall[3] with the positive quadrants of the reference planes. The pancake, a flat volume in the reciprocal lattice containing the recoil momenta of the nuclei, has a well defined distance δ from the origin. δ is the minimum momentum transfer to the nucleus:

$$(1) \qquad \delta = \frac{M}{2 E_o} \cdot \frac{x}{1-x} \quad \text{(in units of Mc)}$$

with $x = k/E_o$, k = photon energy. Main contributions to the intensity come from a thickness δ of the pancake. Distance and thickness of the pancake region are, therefore, functions of x.

The components of a reciprocal lattice vector g in the plane b_2, b_3 have lengths $g_2 = n_2 \cdot \frac{2\pi}{a}$, $g_3 = n_3 \frac{2\pi}{a} \cdot \sqrt{2}$; a = 922 is the edge of the fundamental cube in units $\lambda\!\!\!^{-}_c$, the Compton wave length of the electron.

If Θ is small, the pancake region only contains lattice points of the plane b_2, b_3 through the origin (dashed region) because δ is two orders of magnitude smaller than $2\pi/a$. If x or Θ are changed, this pancake intersection loses or gains lattice points, giving rise to sharp discontinuities in intensity, as has been described earlier[5]. In the special cases of $\alpha = 0^o$, 90^o a whole row of points are causing discontinuities simultaneously.

The intensity to be expected, see ref.[5) 7)], is given by:

$$(2) \qquad I_{th}(x,\Theta,\alpha) \equiv \frac{x}{N\bar{\sigma}} \frac{d\sigma}{dx} = \left[1 + (1-x)^2\right]\left[\psi_1(\delta,\Theta,\alpha) + \psi_1^i(\delta)\right] - \frac{2}{3}(1-x)\left[\psi_2(\delta,\Theta,\alpha) + \psi_2^i(\delta)\right],$$

with $d\sigma/dx$ the differential bremsstrahlung cross section, $\bar{\sigma} = Z^2 \cdot 5.795 \cdot 10^{-28}$ cm^2 a universal cross section, N the number of atoms involved. The variation of the functions $\psi^i_{1,2}$ with δ is very small in the electron energy region of interest, as can be derived from ref.[3]. They are, therefore, taken as constant:

$$(3) \qquad \psi_1^i = 18.6 \qquad \psi_2^i = 17.7$$

These functions represent the incoherent contribution to the intensity due to thermal lattice vibrations. The contribution of the atomic electrons is included.

The functions ψ_1, ψ_2 represent the coherent part. They are given in ref.[5] for $\alpha = 90^0$ and in ref.[6] for any α, using an exponentially screened model of the C atom, [7]. We have used here a Hartree-Type screening model, taken from atomic form-factor plots for carbon given in ref.[8]. The screening function

$$(4) \qquad E(g^2) = \frac{[1 - Fe(g)]^2}{g^4} = \frac{1}{(\beta^{-2}+g^2)^2}\,; \qquad = 111 \cdot z^{-1/3}$$

used in ref.[5] has been replaced by the screening function:

$$(5) \qquad H(g^2) = \begin{cases} 1/(g^2 + 1.377 \cdot 10^{-4})^2 & 0 \le g^2 \le 1.126 \\ (0.2193 \ln g^2 + 2.196)/g^4 & 1.126 \le g^2 \le 2.132 \\ -(686.4 \ln g^2 + 4\,195)/g^2 & 2.132 \le g^2 \le 8.521 \\ (0.0899 \ln g^2 + 1.196)/g^4 & 8.521 \le g^2 \le 29.05 \\ (0.2172 \ln g^2 + 1.939)/g^4 & 29.05 \le g^2 \le 74.32 \\ 1/(g^2 + 5.137 \cdot 10^{-4})^2 & 74.32 \le g^2 \le \infty\,, \end{cases}$$

g^2 in units $10^{+4} \cdot \lambda_c^{-2}$. The functions ψ_1, ψ_2 then take the following form, considering only the plane b_2, b_3 through the origin of the inverse lattice:

$$(6) \qquad \begin{cases} \psi_1(\delta,\theta,\alpha) = \dfrac{(2\pi)^2}{a^3}\dfrac{4\delta}{\theta^2}\sum_{(g)} |F|^2 e^{-Ag^2} H(g^2) \dfrac{g_2^2 + g_3^2}{(g_2\cos\alpha + g_3\sin\alpha)^2} \\ \psi_2(\delta,\theta,\alpha) = \dfrac{(2\pi)^2}{a^3}\dfrac{2\delta^2}{\theta^3}\sum_{(g)} |F|^2 e^{-Ag^2} H(g^2) \dfrac{(g_2^2+g_3^2)(g_2\cos\alpha + g_3\sin\alpha - \frac{\delta}{\theta})}{(g_2\cos\alpha + g_3\sin\alpha)^4} \end{cases}$$

where F is the structure factor of the points ($|F|^2 = 4$) and circles ($|F|^2 = 8$) in the reciprocal lattice plane b_2, b_3 shown in Fig. 1; A = 126, taken from ref.[3], represents the square of the mean temperature displacement of the nuclei at room temperature. The sum is taken over values of (g) in the pancake region only.

We measured the number $N(x,\theta,\alpha)$ of symmetrical and slightly unsymmetrical pairs accepted by the detectors per fixed number of monitor units, normalized to the same energy acceptance (2%), as a function of $x = K/E_o$, at fixed values of θ and α. Delayed coincidences, $N_D(x,\theta,\alpha)$ were subtracted (about 10% of prompt coincidences); background counts $N_B(x,\theta,\alpha)$ were subtracted (about 1% in the interval $0,3 \leq x \leq 1,0$, rising to 3% at $x = 0,1$). The number of counts was then corrected for counter losses at small energies $f(x)$ and for the small variation of the pair production cross section $\sigma_p(x)$ with x, so that the experimental bremsstrahlung intensity is defined as

$$(7) \qquad I_{ex}(x,\theta,\alpha) = \left[N(x,\theta,\alpha) - N_D - N_B \right] \cdot \frac{f(x)}{\sigma_p(x)}$$

The total intensity is constant for each spectrum because θ and α are fixed. The correction for counter losses becomes effective for points below 1 Gev electron energy.

The experimental intensity distribution (7) is normalized to the theoretical distribution (2), (6) on the high energy end of the spectrum, where angular and energy averaging effects have no detectable influence.

Figs. 2, 3, 4, 5 show the results for crystal orientations $\alpha = 0^\circ$ $\theta = 3.44$ mrad, $\alpha = 90^\circ$ $\theta = 2.48$ mrad, $\alpha = 1.5^\circ$ $\theta = 50$ mrad, $\alpha = 89^\circ$ $\theta = 50$ mrad. The statistical errors of the experimental points corrected according to equ. (7) are about 3% throughout. All these spectra show an appreciable difference in their low energy part to the theoretical spectra, I_{th} (full line), but there is agreement in the high energy part of the distribution.

There are a number of effects which tend to smooth out the discontinuities of the theoretical spectrum $I_{th}(x)$, which anticipates that energy and angles are well defined. Out of these the energy spread of the electron beam, $< 0,5\%$, and the energy resolution of the detectors, 2%, can be neglected against angular spreads, and have not been

considered here. The small angles Θ in Figs. 2 and 3 have particularly been chosen to study the change of the intensity distribution due to angular averaging. Such angular spreads of electron momenta against the crystal axis are introduced by the primary divergence of the electron beam, by the multiple scattering of electrons in the radiator, by the spread due to the mosaic structure of the crystal, and by possible angular vibrations of the target. These spreads will influence the spectra in two different ways: The distribution of the first two effects is limited by collimation, while this is not the case for the latter two.

Extremely long computer times are needed for the calculation of an angular average, particularly if free parameters of different distributions are involved. Therefore, we used a simplified model of the actual physical situation by neglecting mosaic spread and vibrations and assuming a single distribution for primary divergence and multiple scattering. The angular distribution of electrons is then determined on the following basis: For an infinitely small collimator the angular distribution of electrons which contribute to the spectral intensity is the same as the angular distribution of photons in the bremsstrahlung process against $\vec{p}_o$. For a finite collimation angle, this distribution has to be folded with the collimator width. If ϑ is the angle of $\vec{p}_o$ against the collimator axis, one obtains the following distribution, projected into a plane through the collimator axis:

$$(8) \qquad W(y) = N_K \left[\frac{y + y_K}{\sqrt{1+(y+y_K)^2}} - \frac{y - y_K}{\sqrt{1+(y-y_K)^2}} \right]; \quad y = \vartheta/\vartheta_o,$$

where N_K is a normalizing factor, $\vartheta_o = M/E_o = 0{,}106$ mrad, $y_k = \vartheta_k/\vartheta_o$, ϑ_k the semiangle of collimation. For rotation of the vertical axis we have $\vartheta_k = \Delta\theta_V = 0.2$ mrad, and for rotation of the horizontal axis $\vartheta_k = \Delta\theta_H = 0.125$ mrad, as defined by the collimator aperture and the target extension. The relations between the rotating angles θ_H, θ_V and the orientation angles θ, α are indicated in Fig. 6 on the unit sphere.

We performed a twofold integration of the intensity I_{th} (equ.(2))

with the distribution $W(\gamma)$ (equ. (8)) over θ and α. The result, $\bar{I}_{th}(x)$, is shown in Figs. 2a, 3a, 4a, 5a. It is important to notice that while averaging over θ only smoothes the spectrum, averaging over α causes the discontinuities to disintegrate into a great number of unresolved peaks. Particularly for $x \ll 1$ new points from the axis perpendicular to $\vec{p}_o$, $\vec{b}_1$ come into the pancake region giving rise to the intensity enhancement near x = 0,05 in Figs. 2a and 3a. This effect is the more pronounced the smaller θ is, because the spread $\Delta\alpha$ is roughly $\Delta\alpha \approx \pm \frac{\Delta\theta}{\theta}$. According to the simplified assumptions, the fit of the averaged intensity to the experimental points is not equally good in all four cases. The high intensity in the valley between the first and second line in Fig. 2a may be due to indirect excitation of the forbidden line $n_2 = 2$.

In Figs. 2a, 3a, 4a, 5a the result of calculated intensity is indicated for the two cases (1) $H(g^2)$ (full line) and (2) $E(g^2)$ (dashed line). The dashed line is shown only where it differs appreciably from case (1). The agreement of the experimental points with the Hartree screening potential is obvious and not surprising, as the latter represents a closer approximation to the charge distribution of electrons. The coincidence of both cases in Fig. 5a is explained by the fact that, as will be shown below, this spectrum is due to the single inverse lattice point $(n_2, n_3) = (1,0)$ for which the two screening functions are nearly equal: $H(g^2_{4,0}) = 1.01 \cdot 10^6$, $E(g^2_{4,0}) = 0.98 \cdot 10^6$. For the spectrum in Fig. 4a, which is also due to a single inverse lattice point, namely (0.2), this is not the case: $H(g^2_{0,2}) = 3.29 \cdot 10^6$, $E(g^2_{0,2}) = 2.45 \cdot 10^6$. These two spectra, therefore, are a sensitive test to the type of the atomic screening function to be used.

In Figs. 4, 4a and 5, 5a we give an example of spectra which we obtained by taking a large θ, θ = 50 mrad, and a small value of α or its complement. Choosing θ large, the thickness of the intersection region, δ/θ, see Fig. 1, becomes small. Thus, by giving this intersection region a small inclination α against one of the axes b_2 or b_3, only one lattice point is included. The experimental results show that

the resolution is high enough to obtain such spectra where the lattice point nearest to the origin gives the main intensity contribution. Increasing $\delta(x)$, this point is lost, and there is a sharp reduction of intensity. The position x_d of the discontinuities for any α is given by

$$(9) \qquad x_d = 1/\left[1 + \frac{1}{\frac{4\pi}{a}\,\frac{\theta_o E_o}{M}\,(n_2 \cos\alpha + n_3 \sqrt{2}\,\sin\alpha)}\right]$$

The first peaks in the spectra of Figs. 4, 4a and 5, 5a are due to the inverse lattice points $(n_2, n_3) = (0,2)$ and $(4,0)$, respectively.

The advantage of these spectra as compared to spectra with $\alpha = 0$ or 90^o lies in the high polarization of the first peak. The polarization $P_{th}(x)$ with respect to the plane $\vec{p_o}$, b_1, as calculated from the formulas given in ref.[6] but using the Hartree screening model, is shown for each spectrum in Figs. 2a, 3a, 4a, 5a. For the first peak in Figs. 4a and 5a one obtains:

$$(10) \qquad \begin{cases} P_{th} = 75{,}7\ \% \quad (0,2) \\ \\ P_{th} = 71{,}3\ \% \quad (4,0) \end{cases}$$

In contrast, the polarization for the first peak in the spectra represented in Figs. 2a and 3a is only 43,1 % and 16,6 % for the same discontinuity position $k_d = 1{,}44$ Gev. The reason for the high degree of polarization lies in the fact that contributions to the photon line intensity come mainly from one lattice point. In the case of $\alpha = 0^o$, 90^o, however, there will be contributions from a row of lattice points, which add in intensity but which cancel partially with respect to the individual contributions to polarization, as can be seen in ref.[6].

The lower intensity of the "one-line" spectra is matched by a better relation of peak-to-bottom intensity at the discontinuity, which is another experimental advantage. This is particularly true for

the spectrum from the point (0,2), Fig.5. The lack of other peaks also simplifies difference measurements. Measurements of polarization are under way at DESY using the method proposed by Barbiellini et al.[6].

We are indebted to Prof. G. Diambrini for encouraging this investigation, and for discussions. Also, we wish to thank Miss W. Kuffner and Mr. G. Filla for technical help. We thank the members of the machine group of DESY for their continuous efforts and Mr. A.Marxen for the excellent workmanship of the goniometer.

LITERATURE

1) B. Ferretti, Nuovo Cim. 7, 118 (1950)

2) M.L. Ter-Mikaelyan, Zhur.Eksp.i.Theor.Fiz. 25, 296 (1953)

3) H. Überall, P.R. 103, 1055 (1956)

4) G. Barbiellini, G. Bologna, G. Diambrini, G.P. Murtas, Phys.Rev.lett. 8, 112 (1962)

5) G. Barbiellini, G. Bologna, G. Diambrini, G.P. Murtas, Phys.Rev.lett. 8, 454 (1962)

6) G. Barbiellini, G. Bologna, G. Diambrini, G.P. Murtas, Nuovo Cim. 28, 435 (1963)

7) I. Schiff, Phys.Rev. 83, 252 (1951)

8) A.T. Nelms, I. Oppenheim, J.Res. Nat.Bur.Stand. 55, 53 (1955)

LIST OF FIGURES

Fig. 1 Orientation of electron momentum $\vec{p}_o$ in the reciprocal lattice space of the diamond, schematic.

Fig. 2	$\alpha = 0^\circ$	$\theta = 3.44$ mrad	Experimental spectra compared with the theoretical intensity, I_{th} (full line)
Fig. 3	$\alpha = 90^\circ$	$\theta = 2.48$ mrad	
Fig. 4	$\alpha = 1.5^\circ$	$\theta = 50$ mrad	
Fig. 5	$\alpha = 89^\circ$	$\theta = 50$ mrad	

Fig. 2a	$\alpha = 0^\circ$	$\theta = 3.44$ mrad	Experimental spectra compared with the averaged intensity and theoretical polarization ——— Hartree potential ----- Exponential potential
Fig. 3a	$\alpha = 90^\circ$	$\theta = 2.48$ mrad	
Fig. 4a	$\alpha = 1.5^\circ$	$\theta = 50$ mrad	
Fig. 5a	$\alpha = 89^\circ$	$\theta = 50$ mrad	

Fig. 6 Relation between θ, α and θ_H, θ_V ; and area defined by collimation on the unit sphere, schematic.

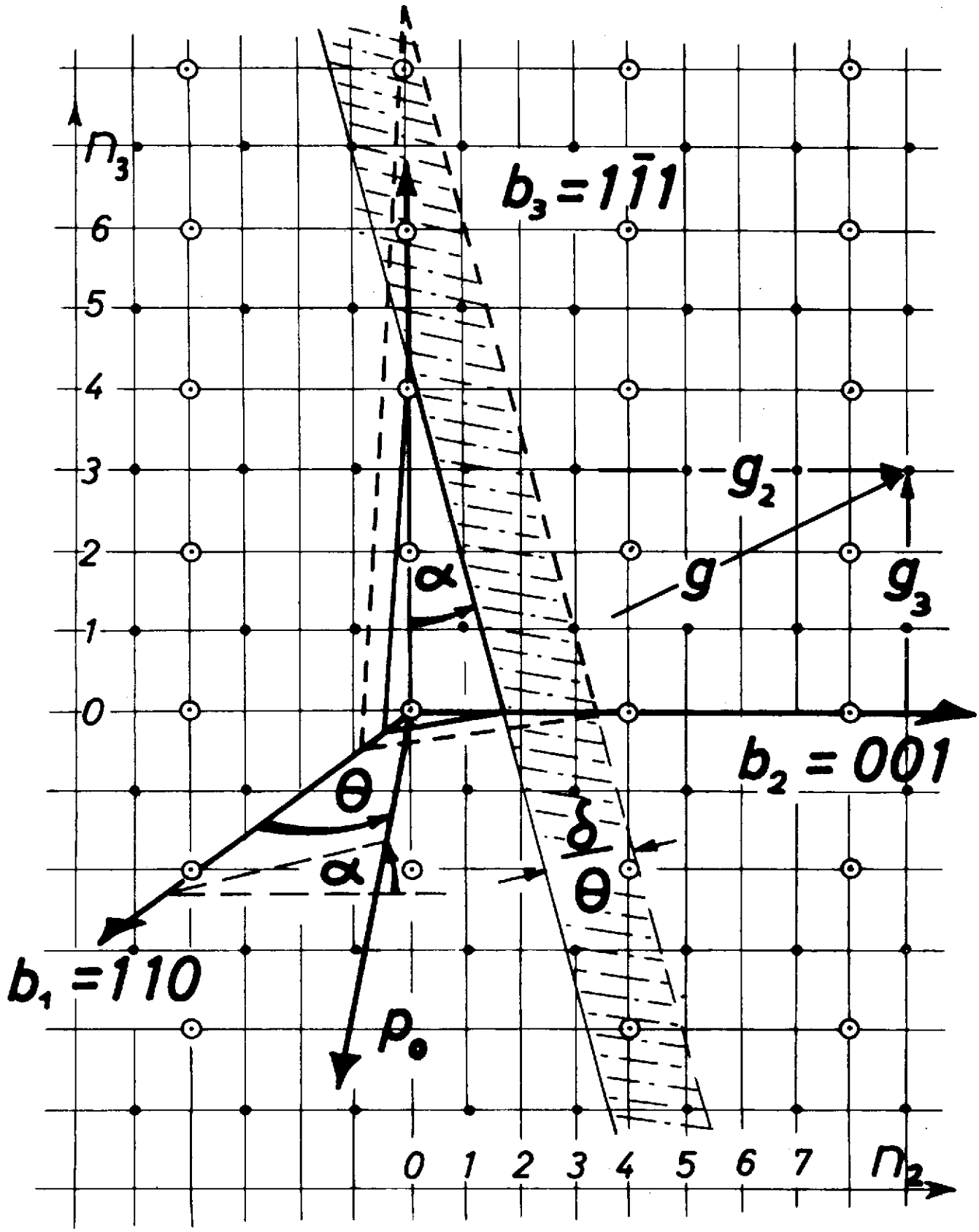

Fig.1 Orientation of electron momentum $\vec{p}_0$ in the reciprocal lattice space of diamond

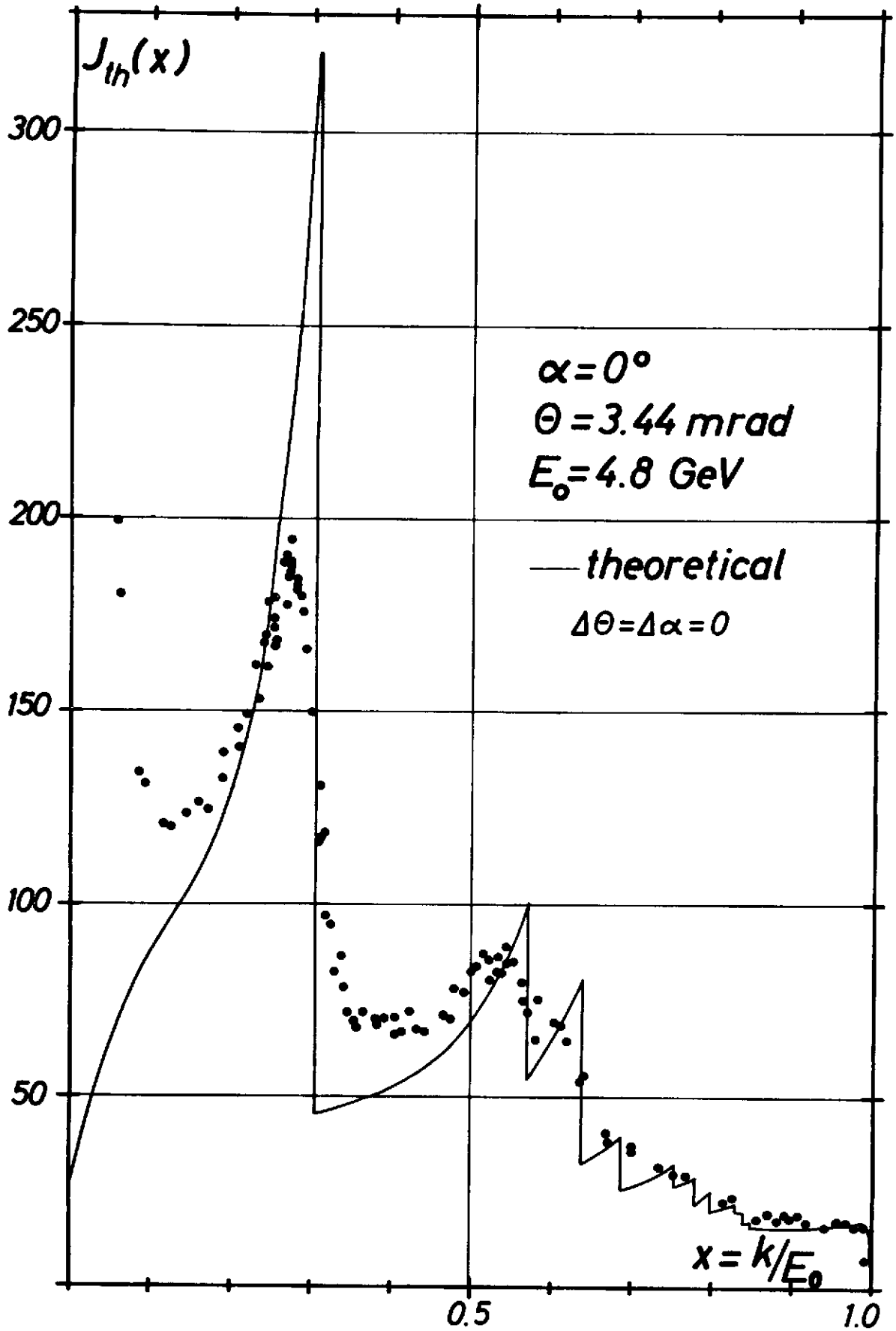

Fig.2 Photon Intensity from Diamond Target

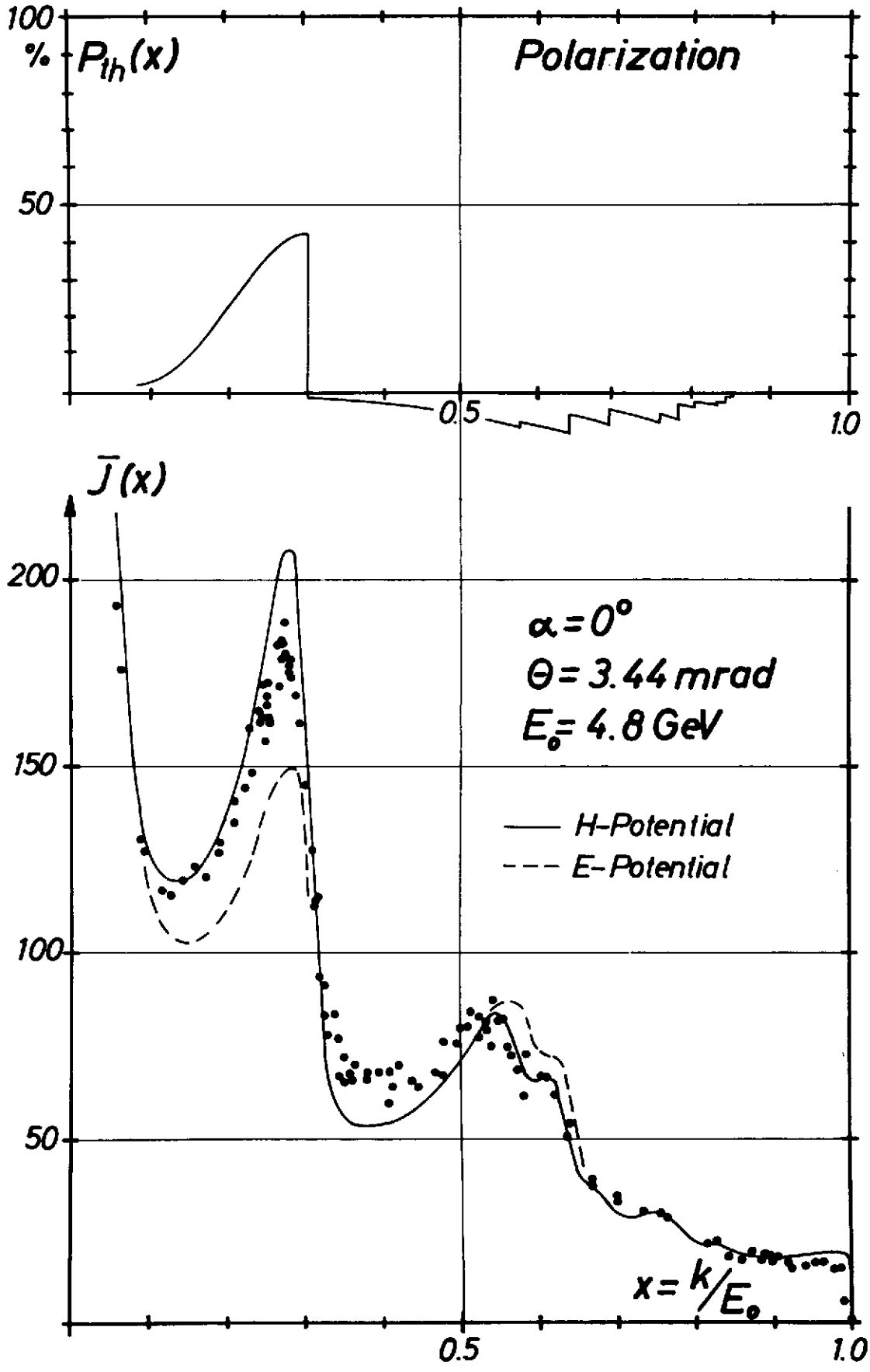

Fig. 2a Photon Intensity and Polarization, Diamond Target

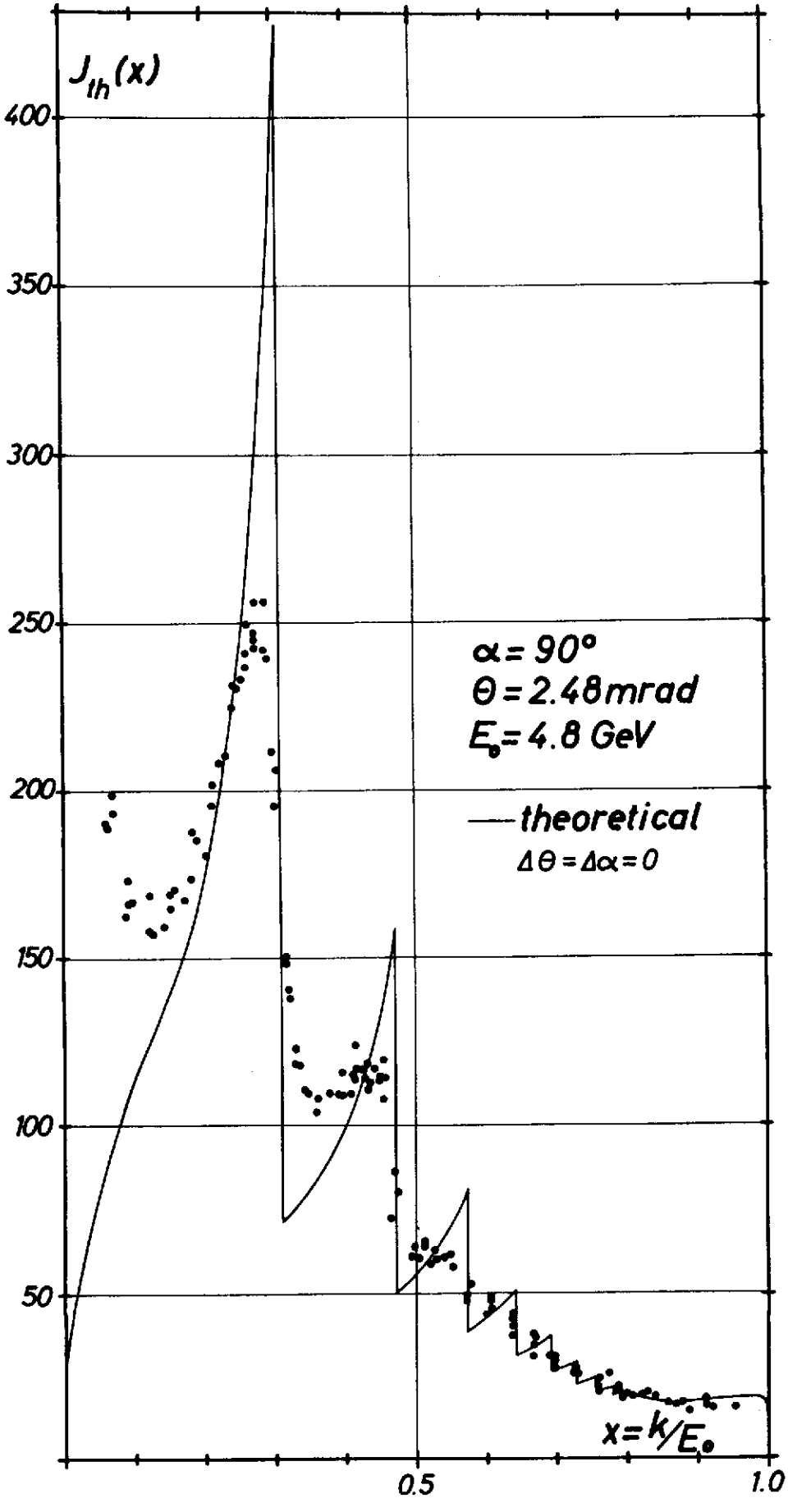

Fig.3 Photon Intensity from Diamond Target

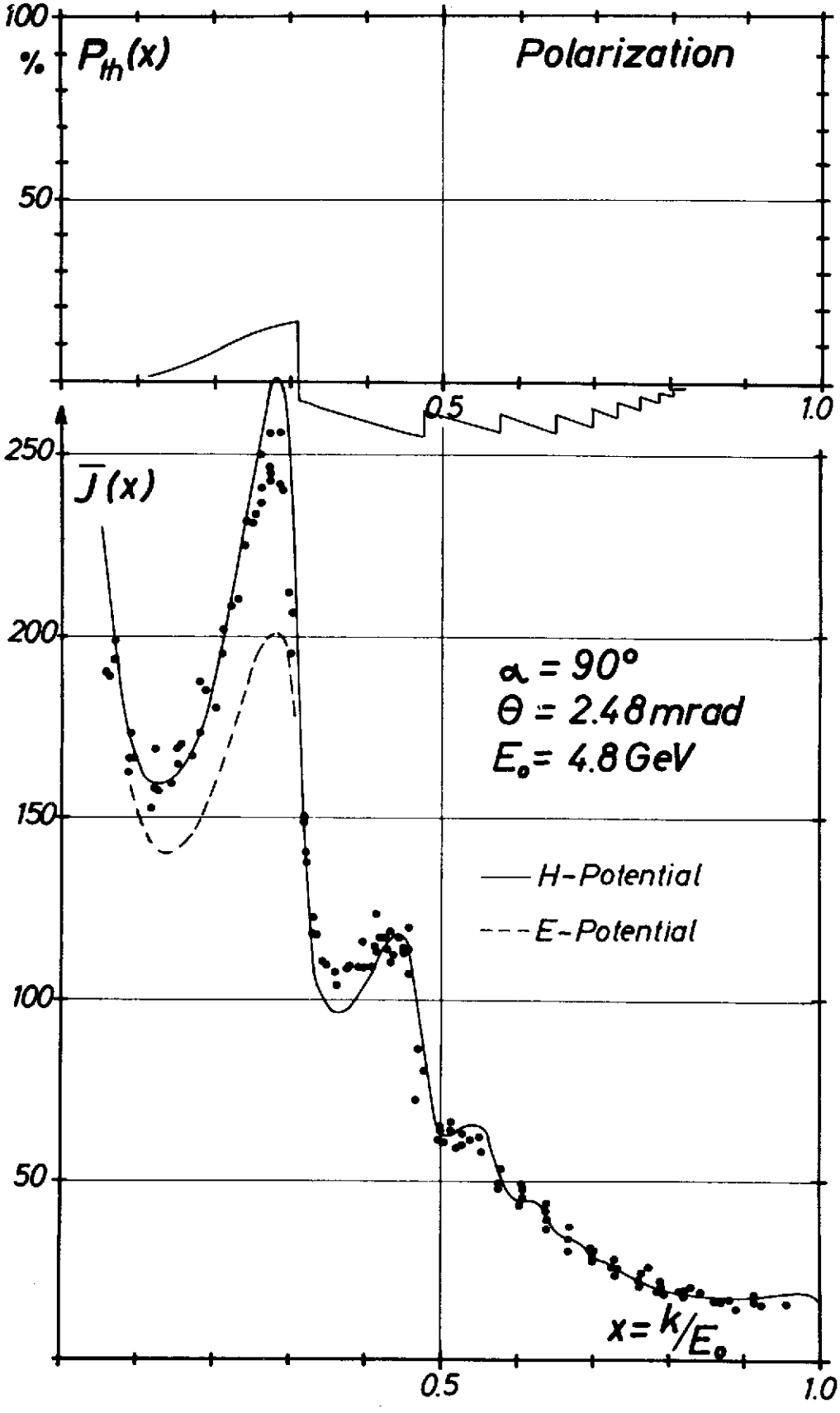

Fig.3a Photon Intensity and Polarization, Diamond Target

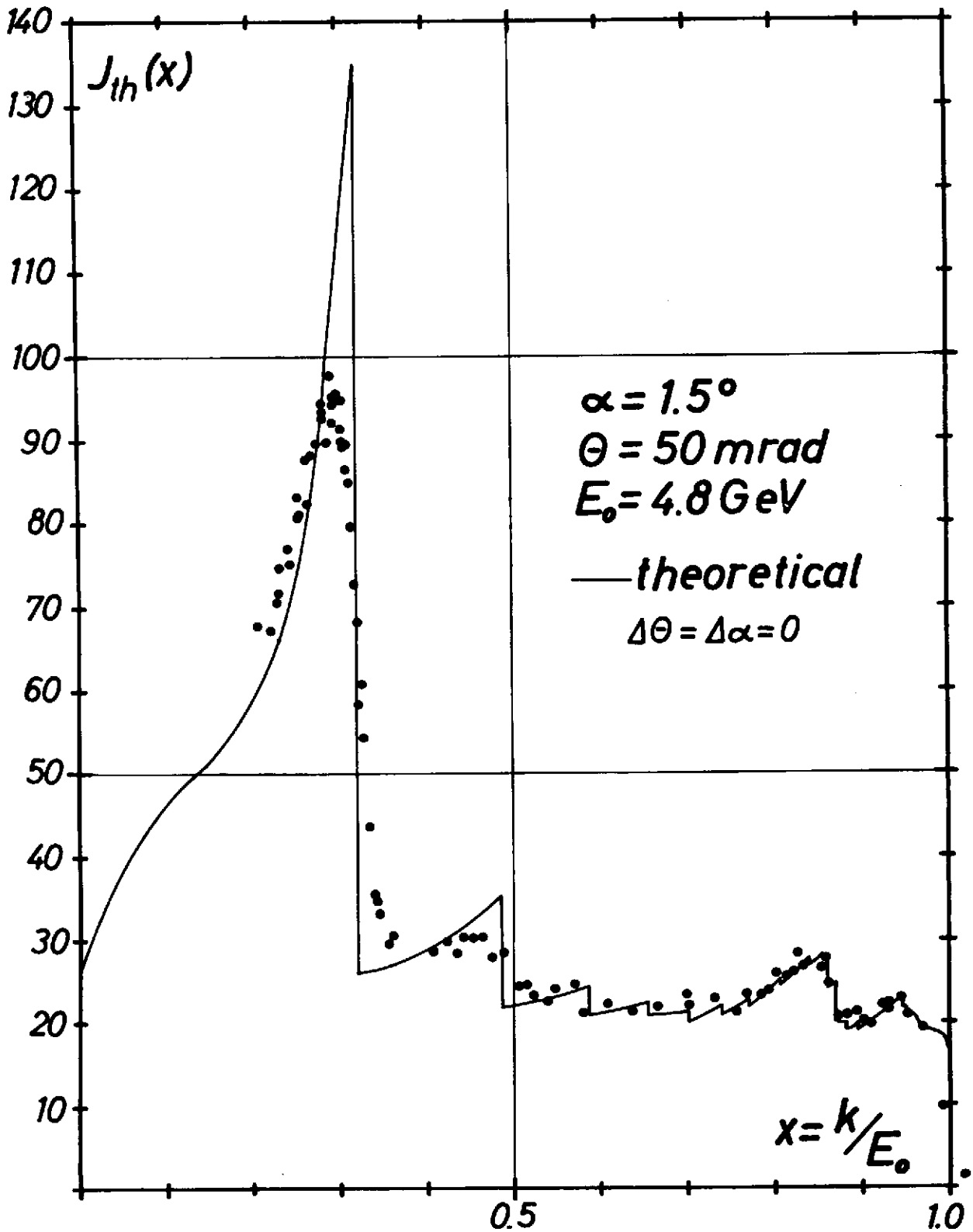

Fig. 4 Photon Intensity from Diamond Target

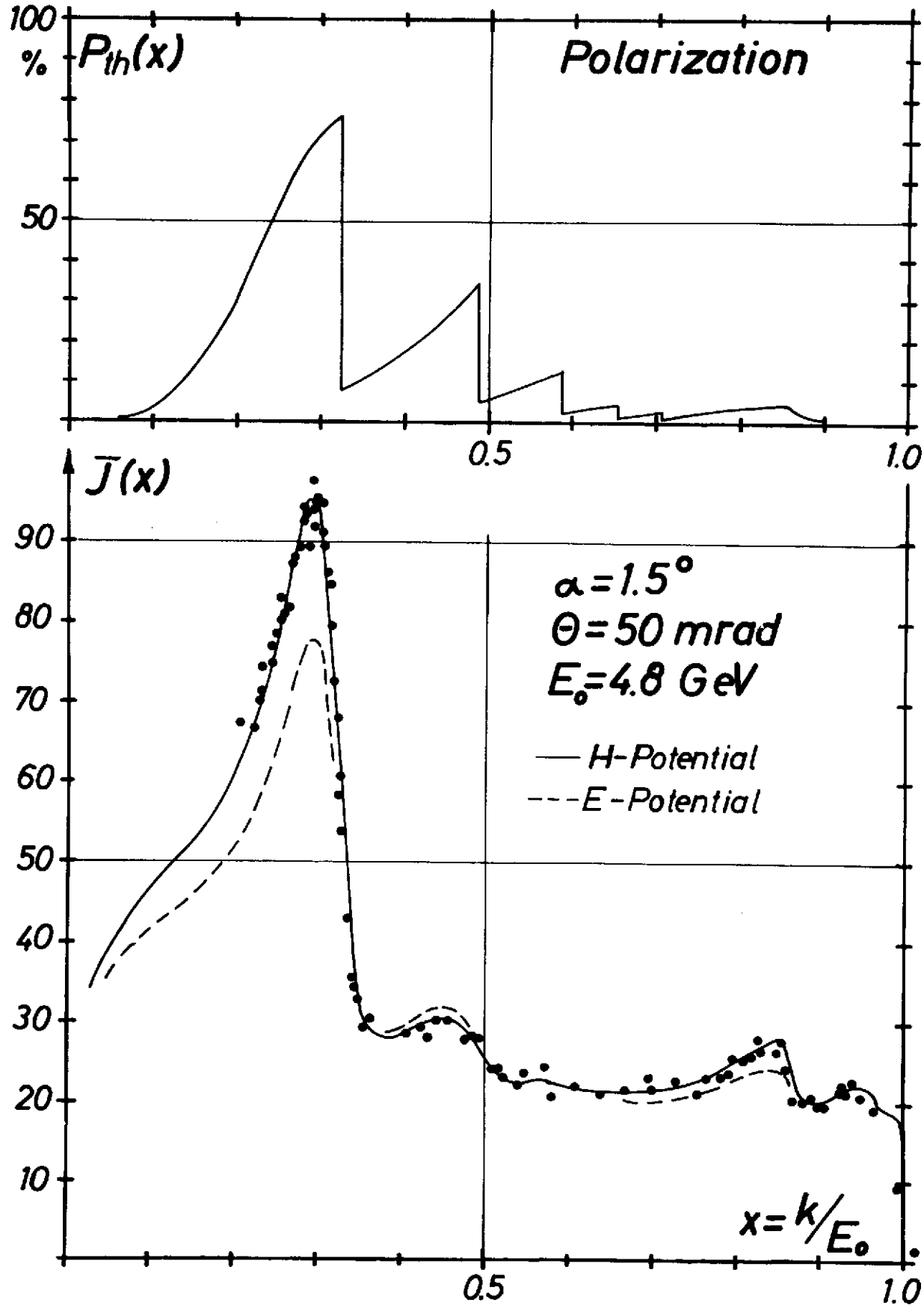

Fig.4a Photon Intensity and Polarization, Diamond Target

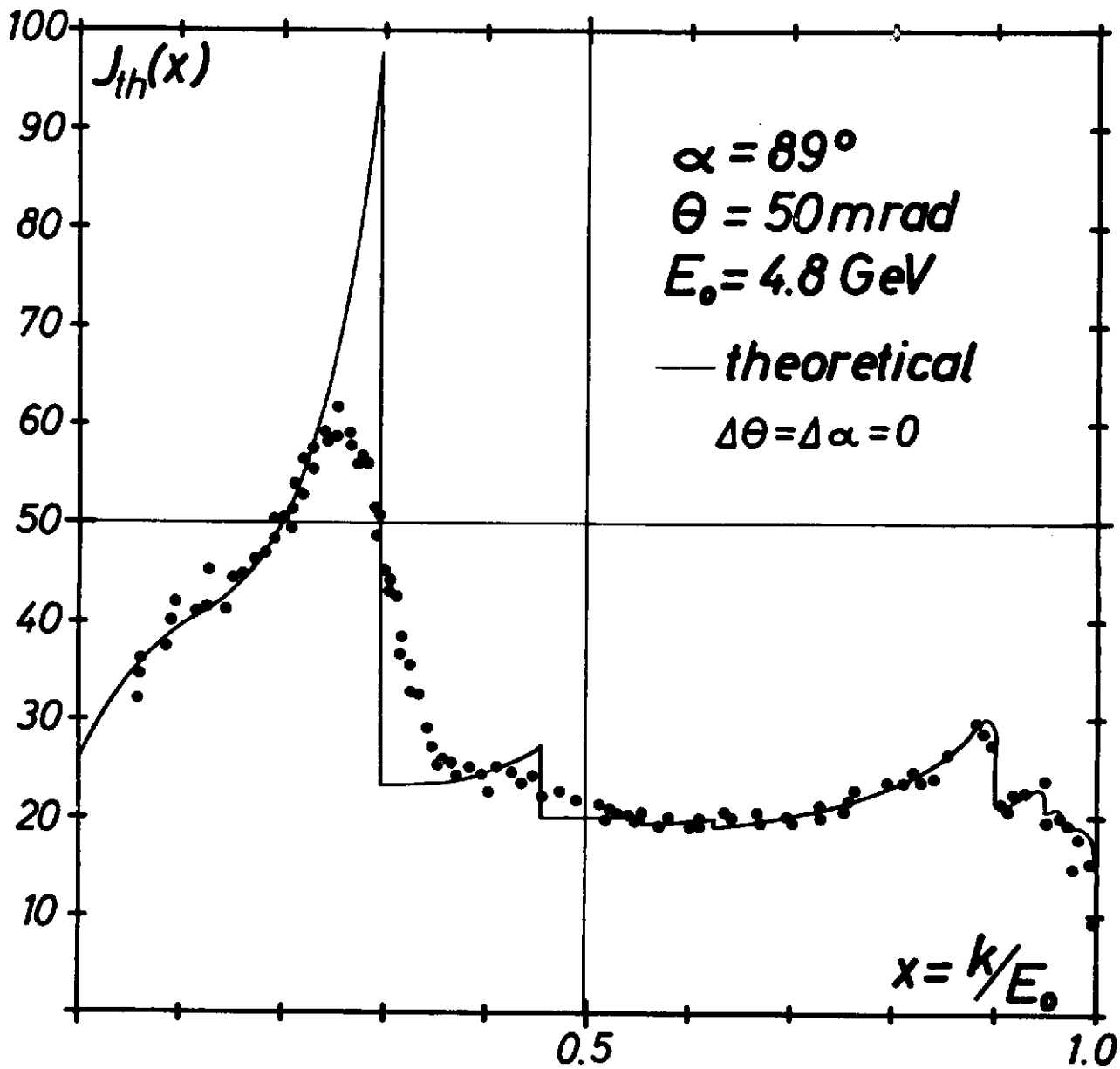

Fig. 5 Photon Intensity from Diamond Target

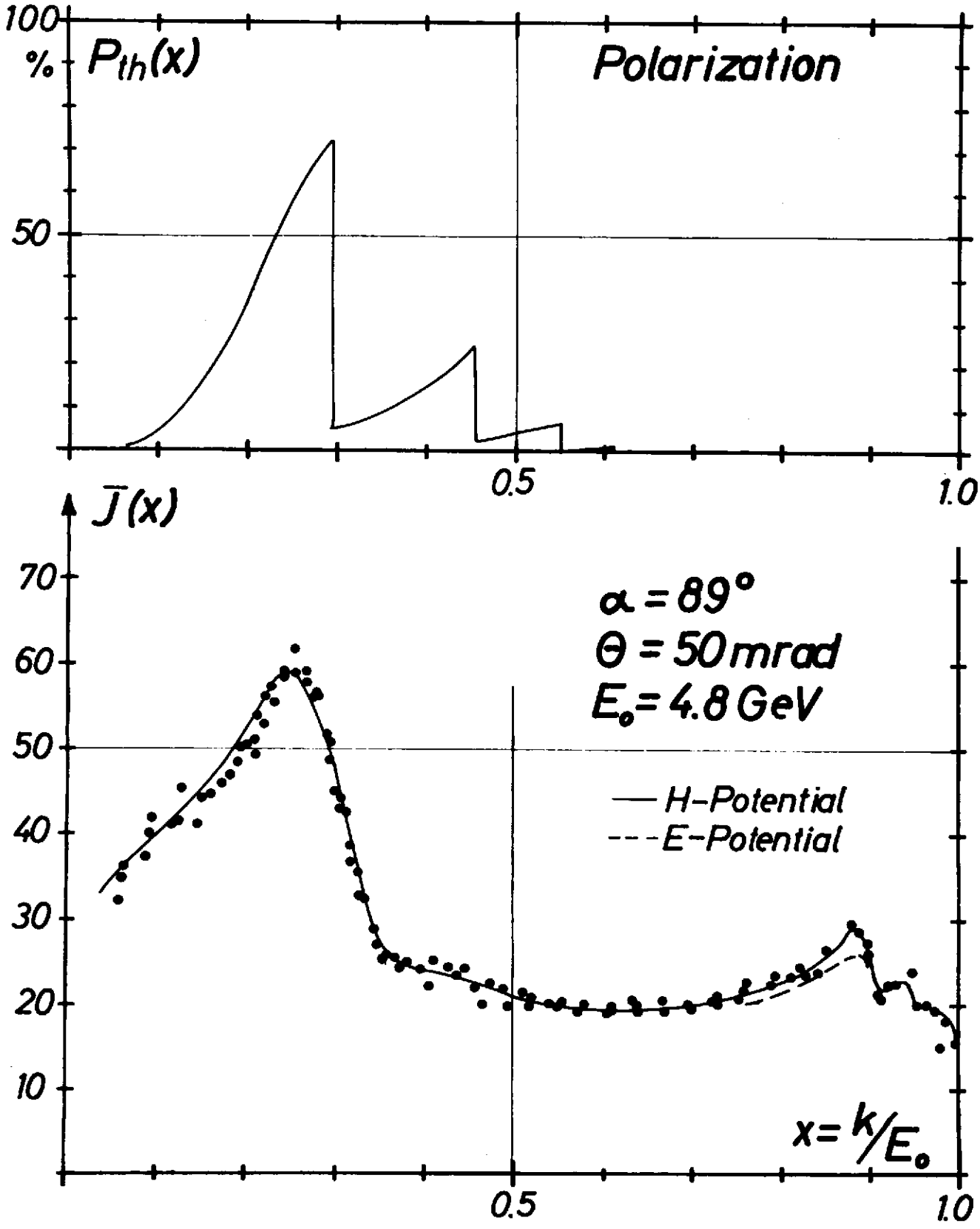

Fig. 5a Photon Intensity and Polarization, Diamond Target

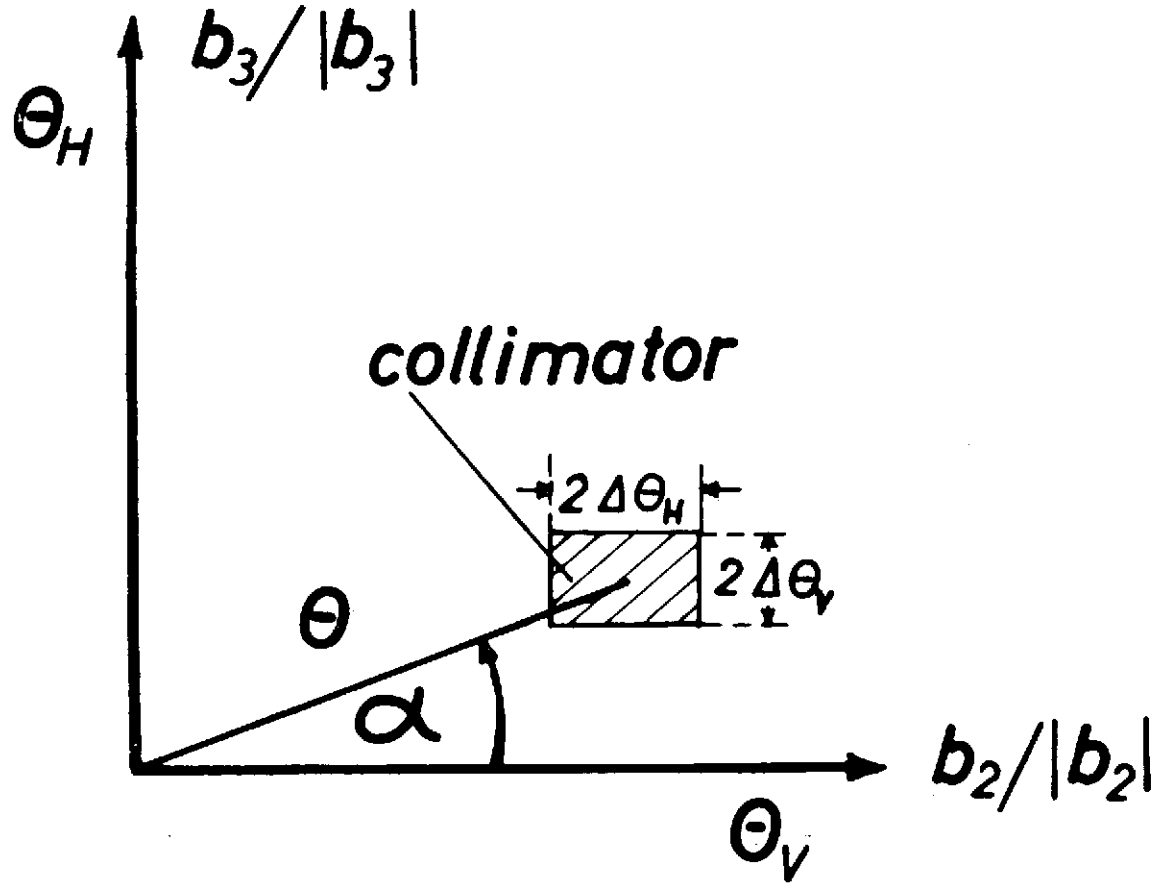

Fig. 6 Relation between Θ, α and Θ_H, Θ_V on unit sphere, schematic